Diagnostic Study

INTERNATIONAL JOURNAL OF SURGERY ONCOLOGY

OPEN

Exploring artificial neural network combined with laser-induced auto-fluorescence technology for noninvasive in vivo upper gastrointestinal tract cancer early diagnosis

Zheng Yi Chen, MBBS[a], Sheng Fu, MBBS, PhD[b,*], Minghui Li, BSc, MSc, PhD[c], Wei Zhang, MBBS[d], Hui Bin Ou, BSc[e]

Abstract

In this study, a laser-induced auto-fluorescence (LIAF) system combined with the artificial neural network (ANN) algorithm is developed for early detection of human upper gastrointestinal tract carcinoma in vivo, through investigating the LIAF spectrum characteristics of the normal mucosa layer and the changes concerning an abnormal surface. Of the 44 participating patients, 41 underwent biopsy at the abnormal surface area at endoscopy. The ANN is employed to differentiate the LIAF data obtained from the normal and carcinoma patients (according to biopsy pathology diagnosis). The LIAF spectrum between 500 and 700 nm is selected and normalized. One data point is selected every 10 nm. A feed-forward back-propagation network with 2 hidden layers is constructed and trained. To evaluate the performance of ANN, 10 normal and 10 carcinoma data sets are tested with the trained ANN. 100% of the carcinoma data are very close to – 1 (desired), 80% of the normal surface is very close to 1 (desired), and 20% return values around – 0.28. Previous works on this type of ANN suggested a threshold of – 0.5. As a result, all normal data are successful and the carcinoma cases are accurately classified and diagnosed. In conclusion, the LIAF technology combined with ANN diagnosis is more accurate.

Keywords: Laser-induced auto-fluorescence, Artificial neural network (ANN) algorithm, Upper gastrointestinal cancers, endoscopy

According to the WHO report, cancer is a leading cause of death worldwide, accounting for 8.8 million deaths in 2015. Within all of the cancers, stomach cancer (754,000 deaths) is the fourth most common cause of cancer mortality. Most of them occur in low-income countries[1]. How to identify the early stage of the gastrointestinal (GI) tract carcinoma and help these patients to have better treatment and better quality of life is still a big challenge worldwide. The laser-induced auto-fluorescence (LIAF) technology has been developed for a few decades for clinical applications[2–5]. In this study, the LIAF technology is used for early identification of human upper GI tract carcinoma. It is a pilot signal endoscopy center study. The aim is to investigate the LIAF spectrum characteristics of the upper GI tract normal mucosa layer and the changes of the spectrum in correlation with the abnormal surface.

Methods

An LIAF spectrum measurement system is built up separately. It consists of a spectrometer (Ocean Optics QEPRO-BUNDLE-FL, preconfigured spectrometer for fluorescence. The spectroscopic range is 350–1000 nm), a 405 nm continuous wave solid laser source (the output power is controlled at 0–20 mW with continuously sweeping), and a Y shape fiber optical bundle with 7 individual fiber optics altogether with the maximum diameter being 2.8 mm, which transmits the laser to the detection area (the maximum output power when coupling to the optical fiber is <0.5 mW) through the operation channel of the endoscope, collects the LIAF spectrum signal, and transmits them to the spectrometer. A personal computer is used to operate the laser source and the LIAF spectrum signal acquisition as well as the raw data storage.

From March to July 2018, 44 patients attended the regular upper GI endoscopy examination at the endoscopy center of the Haikou People's Hospital, Hainan Province, China, who signed the consent to participate in this study. All clinical endoscopy procedures and experimental designs for LIAF followed the preferred reporting of case series in surgery (PROCESS) guidelines which were published by Agha et al in 2018[6]. Forty-one of 44 patients underwent the biopsy at the position of the abnormal surface during the endoscope procedure. The LIAF spectra were

[a]Gastroenterology Department, Haikou People's Hospital, Haikou City, Hainan Province, China, [b]Division of Medicine, Singapore KK Women's and Children's Hospital, Singapore, [c]James Watt School of Engineering, University of Glasgow, Glasgow, UK, Departments of [d]Anaesthesia and [e]Medical Engineering, Haikou People's Hospital, Haikou City, Hainan Province, China

This manuscript has been peer reviewed.

Sponsorships or competing interests that may be relevant to content are disclosed at the end of this article.

*Corresponding author. Address: 100 Bukit Timah Road, Singapore 229899, Singapore. Tel: +65 6394 8402; fax: +65 6394 8941. E-mail address: fu.sheng@kkh.com.sg (S. Fu).

International Journal of Surgery Oncology (2020) 5:e83

Received 27 August 2019; Accepted 13 November 2019

Published online 20 December 2019

http://dx.doi.org/10.1097/IJ9.0000000000000083

taken at the normal surface of the mucosa as well as the abnormal surface before the biopsy was taken. From both the normal and abnormal surface, the LIAF spectrum signals were recorded and analyzed. Some of the data were used for the artificial neural network (ANN) mathematical model training. The rest was used to fit the outcome from the model. The characterized LIAF

Table 1

Comparison for all participations' clinical diagnosis with pathology diagnosis.

Patient Number	Sex	Age (y)	Clincial Diagnosis	Pathology Diagnosis
1	Female	45	No record	(Stomach antrum) changes in chronic active gastritis
2	Female	68	No record	(Stomach antrum) chronic superficial gastritis with erosion
3	Female	37	Gastric ulcer	(Duodenal bulb) mucosal chronic inflammation with erosion
4	Male	49	No record	(Near the junction between of the stomach body and fundus) chronic superficial gastritis
5	Female	77	Stomach lymphoma (cancer)	(Stomach fundus) chronic superficial gastritis
6	Male	71	Duodenal ulcer	(Duodenal bulb) chronic ulcer
7	Female	48	Stomach polyps	(Stomach body) hyperplastic polyps
8	Female	51	Stomach polyps	(Stomach antrum) chronic active gastritis
9	Female	52	Stomach erosion	(Stomach antrum) tubular adenoma, grade I (cancer)
10	Male	45	Erosive gastritis	(Stomach antrum) chronic atrophic gastritis, mild, with activity
11	Male	59	Stomach polyps	1. (Stomach body) fundal gland polyps 2. (Stomach polyps) chronic active gastritis
12	Female	46	Stomach erosion	(Stomach antrum) chronic active gastritis
13	Female	52	Gastric ulcer	(Stomach antrum) chronic atrophic gastritis, mild, with activity
14	Male	76	Gastric ulcer	(lower stomach body parts) chronic active gastritis, with moderate atypical glands, recommended for review after treatment.
15	Female	53	Stomach polyps	(Stomach Fundal) hyperplastic polyps
16	Male	53	Stomach polyps	(Stomach antrum) inflammatory polyps
17	Male	62	Gastric ulcer	(Stomach antrum) changes in chronic active gastritis
18	Male	82	Gastric ulcer	(Stomach antrum) changes in chronic active gastritis
19	Female	67	No record	(Stomach angular) chronic atrophic gastritis (active period) changes
20	Male	67	Gastric ulcer	(Stomach antrum) changes in chronic erosive gastritis
21	Male	81	Erosive gastritis	(Stomach angular) changes in chronic active gastritis, mild atypical hyperplasia of some glandular epithelium, it is recommended to review after treatment
22	Female	53	Stomach xanthelasma	(Stomach antrum) chronic active gastritis with xanthelasma
23	Male	46	Gastric ulcer (suspicion of cancer)	(Stomach antrum) changes in chronic atrophic gastritis
24	Male	57	Gastric ulcer	(Stomach antrum) changes in chronic active gastritis
25	Male	48	Esophageal cancer (postoperative)	1. (Esophageal) squamous cell carcinoma, high-medium differentiation, invades the entire wall of the vessel to the lateral fibrous tissue, and invades blood vessels and nerve bundles. Invasion of cancerous tissue was seen near the margin of the tumor, and no cancer was seen at the margin of the distant tumor 2. (Mucosal stump) mucosal chronic inflammation, with mild atypical squamous epithelium, no cancer 3. Adjacent lymph node metastases (1/1); no lymph node metastases (0/11) 4. (Stomach) chronic atrophic gastritis, mild, no cancer
26	Male	63	Esophageal cancer	(20–30 cm from incisors) squamous cell carcinoma, moderately low differentiation
27	Female	46	stomach polyps	(Stomach body) hyperplastic polyps
28	Male	48	Gastric ulcer	(Stomach angular) chronic ulcers, cannot rule out signet ring cell carcinoma, it is recommended to do immunohistochemistry in our department to confirm the diagnosis
29	Female	50	Stomach polyps	(Stomach angular) hyperplastic polyps
30	Male	77	Normal gastric mucosa	(Stomach antrum) tubular adenoma, grade II
31	Male	68	Stomach angular erosion	(Stomach angular) chronic erosive gastritis
32	Male	64	(Stomach angular) normal gastric mucosa	No biopsy report
33	Male	50	Gastric ulcer	(Stomach antrum) chronic erosive gastritis, focal epithelial mild dysplasia
34	Male	67	Stomach polyps	No biopsy report
35	Female	56	Gastric ulcer (angular)	(Stomach angular) chronic ulcer
36	Male	77	Gastric ulcer	(Stomach antrum) chronic erosive gastritis
37	Male	65	Gastric antral ulcer	(Stomach antrum) chronic active gastritis
38	Male	48	(Stomach angular) ulcer	(Stomach angular) chronic atrophic gastritis, mild, with activity
39	Female	36	Duodenal bulb inflammation	(Duodenal bulb) mucosal chronic inflammation
40	Female	34	Chronic uplift gastritis	(Stomach antrum) chronic active gastritis
41	Male	48	Stomach erosion	(Stomach body) chronic superficial gastritis
42	Male	62	Gastric uplift erosive gastritis	(Stomach antrum) chronic atrophic gastritis, moderate, with activity
43	Male	26	Stomach erosion	No biopsy report
44	Male	67	Esophageal cancer chemotherapy 10 y follow-up	(22 cm from the incisor) squamous epithelium mild dysplasia

spectrum information was linked up with the biopsy pathology microscopy diagnosis report. The correlations of the abnormal surface LIAF spectrum with the pathology diagnoses of the patients were explored and analyzed in details.

Results

More than 2000 LIAF spectra were recorded from 44 patients in this study. Every patient had symptoms and signs. The clinical diagnosis for their disease was not necessarily the same as the pathology diagnosis made on the biopsy histology according to the biopsy pathologic microscopy results from the laboratory. Pathologic diagnosis is the Gold standard for cancer diagnosis in clinical practices at the moment. However, the patient has to wait for a long time after the biopsy sample is sent to the Pathology department. In our department, it may take >2 weeks for the final histology report.

In this study, 17 of 44 were female individuals (38.6%) and 27 were male individuals (61.4%). The mean age for the female patients was 51.1 years old (minimum 34 y old, and maximum 77 y old), whereas for the male patients, the mean age was 60.2 years old (minimum 26 y old, and maximum 82 y old). There were 4 patients (3 female, 1 male) without clinical diagnosis records and 3 patients (all male) without biopsy taken during the endoscopy. Within the clinical diagnoses, 6 patients were diagnosed with cancer. One of them was the esophageal cancer postoperative under chemotherapy 10 years follow-up; 1 was the esophageal cancer postoperative check-up and 1 was just the esophageal cancer. All of them were male. Two females were stomach xanthelasma and lymphoma, respectively. One gastric ulcer suspicion of cancer was male. Others were 8 polyps (5 female individuals and 3 male individuals); 5 stomach erosion (2 female individuals and 3 male individuals); 14 ulcers (1 duodenal male, 1 gastric antral ulcer male, 2 gastric ulcer angular female, and 10 gastric ulcers with 2 female and 8 male). There were 4 gastritis (1 chronic uplift female and 3 erosive male) and 2 normal gastric mucosa males and 1 duodenal bulb inflammation male. Within the pathology diagnosis, also 6 confirmed cases were carcinoma. But 3 of them were different cases with clinical diagnosis. There was a 50% of differentiation rate in between. The ratio would increase if we followed the pathology diagnosis as a gold standard diagnosis. The clinical diagnosis error was 83.3% (5/6). **Table 1** below listed all participated patients' results for comparing the clinical diagnosis with the pathology diagnostic errors.

ANN is employed in this research to differentiate the LIAF spectrum signals obtained from the normal and carcinoma patients (according to biopsy pathology diagnosis report identification) with machine learning and artificial intelligence. The spectrum data between 500 and 700 nm are selected and normalized to the range between 0 and 1. One data point is picked up for every 10 nm in the wavelength, which results in the dimension of a feature vector to be 21. The sample feature vectors extracted from signals corresponding to normal and carcinoma patients are shown in **Figure 1**, and all the 100 feature vectors used for ANN training and testing are provided in the Appendix. A feed-forward back-propagation network with 2 hidden layers of 5 and 1 artificial neurons respectively is constructed, and then trained with 80 feature vectors (40 from normal patients and 40 from carcinoma patients). The desired output value for normal data is set to 1, and the desired output for carcinoma data is set to −1. For the structure and more in-depth discussion of ANN and machine learning, the readers may refer to the literature[7–10] and the references therein. To verify the feasibility of the technique and to evaluate the performance of the ANN, 20 testing feature vectors (10 from normal patients and 10 from carcinoma patients) are inputted to the trained network one by one. The testing results are shown in **Figure 2**. It can be seen from the figure, all the 10 output values corresponding to carcinoma data are very close to −1 (the desired output), 8 of 10 outputs corresponding to normal data are very close to the desired value 1, and 2 outputs get values around −0.28. The threshold between normal and carcinoma classes is a control parameter and must be tweaked and fine-tuned with trails and errors. If the threshold is set to 0 (exactly the middle point between −1 and 1), the successful rate for normal data would be 80%. But some previous studies have suggested a threshold of −0.5, in this case, the successful rate for normal data would be 100%. Note that the successful rate for carcinoma data is always 100%, which means that all the 10 carcinoma data have been accurately classified and diagnosed.

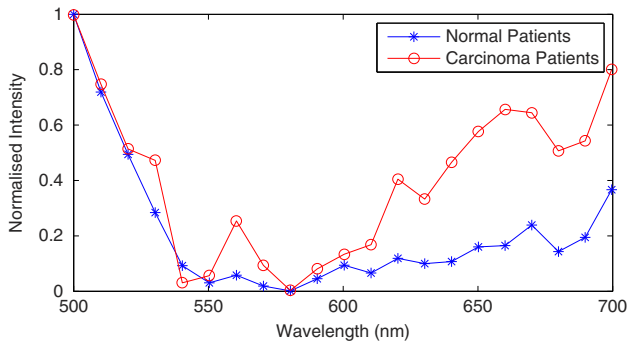

Figure 1. Sample normalized feature vectors extracted from laser-induced autofluorescence spectrum signals corresponding to normal and carcinoma patients.

Comparing with other diagnosis technology and computational methods, the proposed method pairing the ANN algorithm with the LIAF spectrum offers a range of benefits and advantages at both the computational and medical levels. The diagnosis can be performed in real time, since once the neural network is well trained, the extra computational cost of ANN testing is low and minimal, which makes the technology suitable for daily diagnosis and examination at a clinical setup. The ANN training could be slow and time consuming if the training data set is large, however, the training can be performed off-line and for example, in the evening when the diagnosis is not required or using another more powerful workstation. Once the ANN training is complete, the ANN configurations and parameters can be uploaded to the LIAF system. In addition, ANN is a blind machine learning technique,

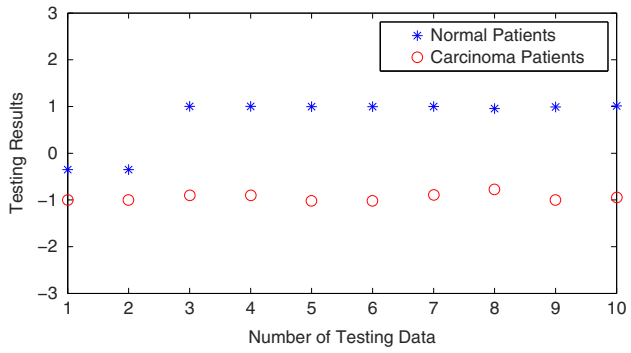

Figure 2. Testing results for normal and carcinoma data with the trained artificial neural network.

which means that the knowledge about the data or the model is not mandatory in the training and testing process, in order to interpret the data. Once the system is setup, a medical doctor without advanced computing and programming skills could perform the diagnosis without any difficulties. In addition, with more and more data sets from the normal and carcinoma patients being collected and involved in the ANN training, the network is potentially becoming more and more mature and the system is supposed to be smart and adaptive to take into account of all the information available, and eventually the diagnosis and examination based on ANN-LIAF will be more accurate.

Conclusions

Six patients with histologically confirmed carcinoma have been used for the ANN studies. All of them were confirmed by our ANN algorithm. The normal mucosa LIAF spectrum was also fit into the hypothesis within the ANN testing, and the results were all confirmed for normal. This pilot study has demonstrated that the LIAF spectrum together with the ANN algorithm for upper GI tract carcinoma diagnosis is superior to the regular traditional endoscope which is under the white light. As mentioned above, the traditional endoscopy procedure necessitates that the doctors need to be skilled endoscopists to identify the type of disease from the screen images. The final diagnosis results depend on the physician's personal experience. Human errors and other mistakes may lead to false diagnoses. This may explain why the clinical diagnosis and the pathology result may not match exactly. In this study, all the ANN results are consistent with the pathology gold standard diagnoses. It can clearly and accurately identify the carcinoma areas noninvasively and in vivo. There is still improvement to be made in this study; for example, the number of patient participants is quite small. We need more patients to further confirm our hypothesis. And we will modify and upgrade our LIAF spectrum system, and add in the ANN algorithm methodology to build an assistant tool for clinical endoscopy procedure practice. It will benefit the patients who are able to obtain their checkup results accurately and more expeditiously with a "light biopsy" and the help of artificial intelligence during their endoscopy. More results will be reported in future studies.

Ethical approval

This study had been approved by the Haikou People's Hospital Bioethics Committee on 23 Sep 2015. Reference No: 2015-014.

Sources of funding

The Science & Technology Department of Hainan Province, China (Grant number: ZDYF2017108).

Authors' contribution

Z.C. is the principal investigator and contributed for grant application and awards the fund. S.F. is the corresponding author. Who is the experimental designer and contributed for system set up and clinical coordinated for this student. He linked up with Haikou People's Hospital, Hainan Provence, China, Singapore KK women's and Children's Hospital and Glasgow University, UK to form the study team and validated the results for LIAF spectra data and ANN analysis compared with the pathologic result. M.L. set up building a mathematical model for this study and using the Artificial Neural Network (ANN) tools to training the spectra experimental data and fit the result to compare with the testing set. All other authors are for participates recruitments, data entrances equipment order, etc.

Conflict of interest disclosures

The authors declare that they have no financial conflict of interest with regard to the content of this report.

Research registration unique identifying number (UIN)

researchregistry5178.

Guarantor

This study supported by the grant of The Science & Technology Department of Hainan Province, China.

Acknowledgments

The authors would like to thank the key research grant support for this study from the Science & Technology Department of Hainan Province, China. Grant number: ZDYF2017108. The authors cannot achieve this result without it.

Appendix

Table A1

Normalized feature vectors corresponding to the normal patients.

1.0000	0.7484	0.5469	0.2570	0.0362	0.0373	0.1211	0.0331	0.0057	0.0369	0.0785	0.0977	0.1190	0.1647	0.1945	0.3159	0.3219	0.4043	0.3015	0.3356	0.5482
1.0000	0.7408	0.5783	0.3726	0.0797	0.0112	0.1189	0.0982	0.0672	0.1349	0.1306	0.0744	0.1547	0.1906	0.2645	0.3812	0.3817	0.4865	0.3139	0.3498	0.6548
1.0000	0.7982	0.6334	0.3415	0.1320	0.0649	0.0485	0.0000	0.1406	0.2469	0.2394	0.0947	0.1441	0.1509	0.2747	0.4310	0.5141	0.5938	0.3923	0.4052	0.5969
1.0000	0.7688	0.5010	0.2749	0.0739	0.0103	0.0976	0.0183	0.0083	0.0684	0.0732	0.0577	0.1257	0.1417	0.1362	0.2081	0.2022	0.3170	0.2308	0.2623	0.4736
1.0000	0.8036	0.5338	0.2909	0.0531	0.0022	0.0765	0.0456	0.0356	0.0711	0.1003	0.1374	0.1935	0.1872	0.2677	0.3756	0.3795	0.4608	0.3349	0.4075	0.6391
1.0000	0.8290	0.5682	0.2738	0.0122	0.0343	0.1652	0.1156	0.0998	0.1166	0.1516	0.1617	0.2748	0.3392	0.3831	0.4688	0.4764	0.5818	0.4618	0.5309	0.8224
1.0000	0.8290	0.5682	0.2738	0.0122	0.0343	0.1652	0.1156	0.0998	0.1166	0.1516	0.1617	0.2748	0.3392	0.3831	0.4688	0.4764	0.5818	0.4618	0.5309	0.8224
1.0000	0.7559	0.4718	0.2248	0.0576	0.0037	0.0279	0.0335	0.0049	0.0260	0.0426	0.0783	0.1656	0.1816	0.2144	0.3634	0.3857	0.4859	0.3736	0.4192	0.6546
1.0000	0.7603	0.5255	0.3012	0.1051	0.0261	0.0582	0.0168	0.0123	0.0900	0.1309	0.1080	0.2178	0.2346	0.2417	0.3624	0.3747	0.4716	0.3887	0.4279	0.6620
1.0000	0.7603	0.5255	0.3012	0.1051	0.0261	0.0582	0.0168	0.0123	0.0900	0.1309	0.1080	0.2178	0.2346	0.2417	0.3624	0.3747	0.4716	0.3887	0.4279	0.6620
1.0000	0.8360	0.6784	0.5264	0.3907	0.3169	0.2941	0.2235	0.1599	0.1327	0.1001	0.0377	0.0446	0.0184	0.0103	0.0350	0.0224	0.0640	0.0128	0.0320	0.1387
1.0000	0.8425	0.6910	0.5220	0.3768	0.2931	0.2662	0.2014	0.1473	0.1284	0.0946	0.0302	0.0414	0.0151	0.0116	0.0364	0.0196	0.0553	0.0045	0.0327	0.1543
1.0000	0.8425	0.6910	0.5220	0.3768	0.2931	0.2662	0.2014	0.1473	0.1284	0.0946	0.0302	0.0414	0.0151	0.0116	0.0364	0.0196	0.0553	0.0045	0.0327	0.1543
1.0000	0.8425	0.6910	0.5220	0.3768	0.2931	0.2662	0.2014	0.1473	0.1284	0.0946	0.0302	0.0414	0.0151	0.0116	0.0364	0.0196	0.0553	0.0045	0.0327	0.1543
1.0000	0.8323	0.6727	0.5106	0.3624	0.2909	0.2795	0.2096	0.1507	0.1397	0.1085	0.0427	0.0485	0.0189	0.0274	0.0584	0.0451	0.0784	0.0061	0.0356	0.1487
1.0000	0.8323	0.6727	0.5106	0.3624	0.2909	0.2795	0.2096	0.1507	0.1397	0.1085	0.0427	0.0485	0.0189	0.0274	0.0584	0.0451	0.0784	0.0061	0.0356	0.1487
1.0000	0.8323	0.6727	0.5106	0.3624	0.2909	0.2795	0.2096	0.1507	0.1397	0.1085	0.0427	0.0485	0.0189	0.0274	0.0584	0.0451	0.0784	0.0061	0.0356	0.1487
1.0000	0.8192	0.6468	0.4757	0.3186	0.2505	0.2414	0.1761	0.1196	0.1088	0.0810	0.0167	0.0358	0.0120	0.0162	0.0558	0.0455	0.0909	0.0261	0.0576	0.1882
1.0000	0.8192	0.6468	0.4757	0.3186	0.2505	0.2414	0.1761	0.1196	0.1088	0.0810	0.0167	0.0358	0.0120	0.0162	0.0558	0.0455	0.0909	0.0261	0.0576	0.1882
1.0000	0.8192	0.6468	0.4757	0.3186	0.2505	0.2414	0.1761	0.1196	0.1088	0.0810	0.0167	0.0358	0.0120	0.0162	0.0558	0.0455	0.0909	0.0261	0.0576	0.1882
1.0000	0.7962	0.5949	0.3662	0.1510	0.0997	0.1517	0.1069	0.0645	0.0878	0.0869	0.0028	0.0425	0.0251	0.0466	0.1083	0.1068	0.1826	0.0992	0.1412	0.3345
1.0000	0.7695	0.5595	0.3132	0.0894	0.0557	0.1401	0.1302	0.1017	0.0980	0.0719	0.0025	0.0822	0.0610	0.0834	0.1783	0.1932	0.2673	0.1445	0.2271	0.4787
1.0000	0.7695	0.5595	0.3132	0.0894	0.0557	0.1401	0.1302	0.1017	0.0980	0.0719	0.0025	0.0822	0.0610	0.0834	0.1783	0.1932	0.2673	0.1445	0.2271	0.4787
1.0000	0.7695	0.5595	0.3132	0.0894	0.0557	0.1401	0.1302	0.1017	0.0980	0.0719	0.0025	0.0822	0.0610	0.0834	0.1783	0.1932	0.2673	0.1445	0.2271	0.4787
1.0000	0.7743	0.5365	0.3031	0.0618	0.0110	0.1328	0.1285	0.1371	0.2092	0.2254	0.1520	0.2407	0.2234	0.2578	0.3419	0.3369	0.4339	0.3041	0.3932	0.6568
1.0000	0.7743	0.5365	0.3031	0.0618	0.0110	0.1328	0.1285	0.1371	0.2092	0.2254	0.1520	0.2407	0.2234	0.2578	0.3419	0.3369	0.4339	0.3041	0.3932	0.6568
1.0000	0.7743	0.5365	0.3031	0.0618	0.0110	0.1328	0.1285	0.1371	0.2092	0.2254	0.1520	0.2407	0.2234	0.2578	0.3419	0.3369	0.4339	0.3041	0.3932	0.6568
1.0000	0.7531	0.5301	0.2894	0.0323	0.0242	0.1339	0.1172	0.1333	0.1908	0.2084	0.1715	0.2680	0.2965	0.3253	0.4152	0.4095	0.5189	0.3742	0.4527	0.7428
1.0000	0.7531	0.5301	0.2894	0.0323	0.0242	0.1339	0.1172	0.1333	0.1908	0.2084	0.1715	0.2680	0.2965	0.3253	0.4152	0.4095	0.5189	0.3742	0.4527	0.7428
1.0000	0.7531	0.5301	0.2894	0.0323	0.0242	0.1339	0.1172	0.1333	0.1908	0.2084	0.1715	0.2680	0.2965	0.3253	0.4152	0.4095	0.5189	0.3742	0.4527	0.7428
1.0000	0.7194	0.4941	0.2841	0.0926	0.0306	0.0579	0.0189	0.0013	0.0450	0.0941	0.0657	0.1187	0.0998	0.1070	0.1601	0.1649	0.2392	0.1433	0.1945	0.3663
1.0000	0.7684	0.5858	0.3500	0.1230	0.0556	0.0740	0.0376	0.0017	0.0394	0.0870	0.0409	0.1207	0.1129	0.1350	0.2182	0.2382	0.3613	0.2541	0.2892	0.4622
1.0000	0.7658	0.5992	0.3426	0.0894	0.0229	0.0739	0.0312	0.0054	0.0348	0.0489	0.0163	0.1102	0.1068	0.1010	0.1575	0.1548	0.2401	0.0973	0.1193	0.3521
1.0000	0.8137	0.6621	0.4752	0.2988	0.2252	0.2457	0.1743	0.0842	0.0467	0.0377	0.0022	0.0866	0.1382	0.1930	0.2375	0.2474	0.3501	0.2543	0.2998	0.5164
1.0000	0.7590	0.5538	0.3397	0.1441	0.0806	0.1015	0.0301	0.0049	0.0405	0.0515	0.0018	0.0615	0.0552	0.0951	0.1775	0.1972	0.2818	0.1956	0.2514	0.4561
1.0000	0.7590	0.5538	0.3397	0.1441	0.0806	0.1015	0.0301	0.0049	0.0405	0.0515	0.0018	0.0615	0.0552	0.0951	0.1775	0.1972	0.2818	0.1956	0.2514	0.4561
1.0000	0.7307	0.5318	0.2998	0.0912	0.0185	0.0684	0.0279	0.0032	0.0424	0.0353	0.0020	0.0973	0.1268	0.1633	0.2293	0.2304	0.3267	0.2147	0.2556	0.4453
1.0000	0.7307	0.5318	0.2998	0.0912	0.0185	0.0684	0.0279	0.0032	0.0424	0.0353	0.0020	0.0973	0.1268	0.1633	0.2293	0.2304	0.3267	0.2147	0.2556	0.4453
1.0000	0.7737	0.5671	0.3348	0.1082	0.0346	0.0828	0.0574	0.0299	0.0587	0.0728	0.0009	0.0748	0.0714	0.1081	0.2001	0.2188	0.2942	0.1878	0.2157	0.3861
1.0000	0.7137	0.5193	0.3239	0.0767	0.0392	0.1032	0.0393	0.0049	0.0355	0.0634	0.0082	0.1210	0.1476	0.1647	0.2373	0.2423	0.3496	0.2676	0.3096	0.4929
1.0000	0.7924	0.6436	0.4807	0.3063	0.2178	0.1988	0.1266	0.0710	0.0813	0.0824	0.0100	0.0174	0.0084	0.0189	0.0478	0.0353	0.0874	0.0411	0.0933	0.2304
1.0000	0.8258	0.6427	0.4375	0.2368	0.1452	0.1399	0.1370	0.0912	0.0810	0.0698	0.0370	0.0674	0.0442	0.0212	0.0540	0.0131	0.0773	0.0210	0.0544	0.1799
1.0000	0.8258	0.6427	0.4375	0.2368	0.1452	0.1399	0.1370	0.0912	0.0810	0.0698	0.0370	0.0674	0.0442	0.0212	0.0540	0.0131	0.0773	0.0210	0.0544	0.1799
1.0000	0.8306	0.6808	0.4971	0.3331	0.2685	0.2578	0.1646	0.1235	0.1667	0.1319	0.0446	0.0534	0.0146	0.0147	0.0478	0.0393	0.1135	0.0950	0.1180	0.2652
1.0000	0.8091	0.6826	0.5221	0.3286	0.2194	0.2232	0.1404	0.0733	0.0624	0.0588	0.0015	0.0308	0.0153	0.0269	0.0652	0.0775	0.1217	0.0457	0.1285	0.2695
1.0000	0.8091	0.6826	0.5221	0.3286	0.2194	0.2232	0.1404	0.0733	0.0624	0.0588	0.0015	0.0308	0.0153	0.0269	0.0652	0.0775	0.1217	0.0457	0.1285	0.2695
1.0000	0.8020	0.6552	0.5072	0.2879	0.1830	0.1850	0.1342	0.1029	0.0770	0.0592	0.0024	0.0241	0.0339	0.0364	0.0482	0.0412	0.1056	0.0712	0.1023	0.2063
1.0000	0.8040	0.6700	0.5331	0.3892	0.3171	0.3319	0.2360	0.1402	0.1045	0.0616	0.0023	0.0244	0.0300	0.0036	0.0198	0.0175	0.0640	0.0244	0.0617	0.1628
1.0000	0.8040	0.6700	0.5331	0.3892	0.3171	0.3319	0.2360	0.1402	0.1045	0.0616	0.0023	0.0244	0.0300	0.0036	0.0198	0.0175	0.0640	0.0244	0.0617	0.1628
1.0000	0.8487	0.7246	0.5761	0.3949	0.2805	0.2458	0.1662	0.1050	0.0818	0.0571	0.0077	0.0320	0.0113	0.0039	0.0423	0.0412	0.1181	0.0916	0.1097	0.2183

Each row of the data represents one feature vector with 21 elements. The laser-induced auto-fluorescence spectrum data between 500 and 700 nm are selected and normalized to the range between 0 and 1. One data point is picked up for every 10 nm in the wavelength, which results in the dimension of a feature vector to be 21.

Table A2

Normalized feature vectors corresponding to the carcinoma patients.

0.8898	0.7870	0.7161	0.3957	0.0615	0.0141	0.1682	0.1642	0.1504	0.2186	0.2622	0.1667	0.2992	0.3137	0.4002	0.5569	0.5796	0.7087	0.5447	0.6328	1.0000
0.8898	0.7870	0.7161	0.3957	0.0615	0.0141	0.1682	0.1642	0.1504	0.2186	0.2622	0.1667	0.2992	0.3137	0.4002	0.5569	0.5796	0.7087	0.5447	0.6328	1.0000
0.6874	0.6033	0.4090	0.2090	0.0215	0.0277	0.1492	0.0859	0.0421	0.1049	0.1573	0.1114	0.2836	0.3186	0.3856	0.5180	0.5456	0.6965	0.5703	0.6787	1.0000
0.6874	0.6033	0.4090	0.2090	0.0215	0.0277	0.1492	0.0859	0.0421	0.1049	0.1573	0.1114	0.2836	0.3186	0.3856	0.5180	0.5456	0.6965	0.5703	0.6787	1.0000
0.6874	0.6033	0.4090	0.2090	0.0215	0.0277	0.1492	0.0859	0.0421	0.1049	0.1573	0.1114	0.2836	0.3186	0.3856	0.5180	0.5456	0.6965	0.5703	0.6787	1.0000
0.6874	0.6033	0.4090	0.2090	0.0215	0.0277	0.1492	0.0859	0.0421	0.1049	0.1573	0.1114	0.2836	0.3186	0.3856	0.5180	0.5456	0.6965	0.5703	0.6787	1.0000
0.6874	0.6033	0.4090	0.2090	0.0215	0.0277	0.1492	0.0859	0.0421	0.1049	0.1573	0.1114	0.2836	0.3186	0.3856	0.5180	0.5456	0.6965	0.5703	0.6787	1.0000
0.6874	0.6033	0.4090	0.2090	0.0215	0.0277	0.1492	0.0859	0.0421	0.1049	0.1573	0.1114	0.2836	0.3186	0.3856	0.5180	0.5456	0.6965	0.5703	0.6787	1.0000
0.6874	0.6033	0.4090	0.2090	0.0215	0.0277	0.1492	0.0859	0.0421	0.1049	0.1573	0.1114	0.2836	0.3186	0.3856	0.5180	0.5456	0.6965	0.5703	0.6787	1.0000
0.6874	0.6033	0.4090	0.2090	0.0215	0.0277	0.1492	0.0859	0.0421	0.1049	0.1573	0.1114	0.2836	0.3186	0.3856	0.5180	0.5456	0.6965	0.5703	0.6787	1.0000
1.0000	0.8186	0.5779	0.3080	0.1226	0.0260	0.0670	0.0215	0.0211	0.1226	0.1696	0.1634	0.2381	0.2207	0.2270	0.3205	0.3222	0.3954	0.3471	0.4069	0.5356
1.0000	0.8186	0.5779	0.3080	0.1226	0.0260	0.0670	0.0215	0.0211	0.1226	0.1696	0.1634	0.2381	0.2207	0.2270	0.3205	0.3222	0.3954	0.3471	0.4069	0.5356
1.0000	0.8170	0.6084	0.3228	0.0602	0.0238	0.0858	0.0698	0.0870	0.1430	0.2356	0.2038	0.3111	0.2733	0.2742	0.3576	0.3309	0.4460	0.3499	0.4114	0.6572
1.0000	0.8170	0.6084	0.3228	0.0602	0.0238	0.0858	0.0698	0.0870	0.1430	0.2356	0.2038	0.3111	0.2733	0.2742	0.3576	0.3309	0.4460	0.3499	0.4114	0.6572
1.0000	0.8256	0.5878	0.3221	0.0956	0.0137	0.0549	0.0108	0.0443	0.1859	0.2453	0.2371	0.2793	0.2638	0.2542	0.2931	0.2905	0.3150	0.2345	0.2741	0.5055
1.0000	0.8256	0.5878	0.3221	0.0956	0.0137	0.0549	0.0108	0.0443	0.1859	0.2453	0.2371	0.2793	0.2638	0.2542	0.2931	0.2905	0.3150	0.2345	0.2741	0.5055
1.0000	0.7861	0.5771	0.3011	0.0376	0.0252	0.0339	0.0117	0.0046	0.0980	0.1992	0.2265	0.3749	0.3423	0.3768	0.4713	0.4763	0.5959	0.5460	0.6119	0.7487
1.0000	0.8126	0.6178	0.3237	0.0601	0.0074	0.0550	0.0524	0.0873	0.1669	0.2989	0.3099	0.4377	0.3974	0.4161	0.4730	0.4937	0.5740	0.4583	0.4357	0.7052
0.9797	0.8029	0.6249	0.3913	0.0910	0.0397	0.0886	0.0390	0.0132	0.1470	0.3598	0.4091	0.5167	0.4847	0.5608	0.6632	0.6902	0.8366	0.7750	0.8279	0.9963
0.9797	0.8029	0.6249	0.3913	0.0910	0.0397	0.0886	0.0390	0.0132	0.1470	0.3598	0.4091	0.5167	0.4847	0.5608	0.6632	0.6902	0.8366	0.7750	0.8279	0.9963
0.2403	0.3723	0.3074	0.2300	0.1300	0.0530	0.0820	0.0185	0.0026	0.0745	0.1848	0.2469	0.4157	0.4657	0.5771	0.6997	0.7381	0.8252	0.7650	0.8119	0.9954
0.2403	0.3723	0.3074	0.2300	0.1300	0.0530	0.0820	0.0185	0.0026	0.0745	0.1848	0.2469	0.4157	0.4657	0.5771	0.6997	0.7381	0.8252	0.7650	0.8119	0.9954
0.3884	0.3994	0.3183	0.2105	0.0814	0.0497	0.1118	0.0611	0.0041	0.0489	0.1376	0.1761	0.3401	0.4371	0.5643	0.6607	0.7185	0.7960	0.7584	0.8235	0.9976
0.3884	0.3994	0.3183	0.2105	0.0814	0.0497	0.1118	0.0611	0.0041	0.0489	0.1376	0.1761	0.3401	0.4371	0.5643	0.6607	0.7185	0.7960	0.7584	0.8235	0.9976
0.3598	0.3194	0.2610	0.1771	0.0238	0.0215	0.0541	0.0302	0.0178	0.0690	0.1818	0.2243	0.3968	0.4587	0.5680	0.6861	0.7228	0.7918	0.7354	0.8233	0.9964
0.3598	0.3194	0.2610	0.1771	0.0238	0.0215	0.0541	0.0302	0.0178	0.0690	0.1818	0.2243	0.3968	0.4587	0.5680	0.6861	0.7228	0.7918	0.7354	0.8233	0.9964
0.3652	0.3455	0.2930	0.2046	0.0661	0.0299	0.0931	0.0586	0.0559	0.1427	0.1949	0.2605	0.3469	0.4685	0.5781	0.7017	0.7618	0.8376	0.8172	0.8806	1.0000
0.3652	0.3455	0.2930	0.2046	0.0661	0.0299	0.0931	0.0586	0.0559	0.1427	0.1949	0.2605	0.3469	0.4685	0.5781	0.7017	0.7618	0.8376	0.8172	0.8806	1.0000
0.2865	0.3918	0.3288	0.1814	0.0508	0.0013	0.0733	0.0465	0.0027	0.1021	0.2067	0.2324	0.4082	0.4831	0.5824	0.6892	0.7179	0.8183	0.7840	0.8628	0.9965
0.2865	0.3918	0.3288	0.1814	0.0508	0.0013	0.0733	0.0465	0.0027	0.1021	0.2067	0.2324	0.4082	0.4831	0.5824	0.6892	0.7179	0.8183	0.7840	0.8628	0.9965
0.9982	0.7472	0.5135	0.4724	0.0303	0.0566	0.2536	0.0935	0.0029	0.0809	0.1335	0.1679	0.4049	0.3328	0.4654	0.5766	0.6566	0.6447	0.5067	0.5431	0.8007
1.0000	0.8127	0.6169	0.4104	0.0164	0.0623	0.0975	0.0589	0.0326	0.1814	0.2449	0.1207	0.3296	0.2651	0.3267	0.4019	0.3391	0.4399	0.4223	0.4587	0.7190
1.0000	0.7778	0.4875	0.3413	0.0800	0.0003	0.1076	0.0474	0.0254	0.1449	0.2267	0.1038	0.2657	0.3684	0.3517	0.4436	0.4379	0.6449	0.5234	0.5686	0.9257
1.0000	0.7778	0.4875	0.3413	0.0800	0.0003	0.1076	0.0474	0.0254	0.1449	0.2267	0.1038	0.2657	0.3684	0.3517	0.4436	0.4379	0.6449	0.5234	0.5686	0.9257
0.9731	0.8311	0.5704	0.3346	0.1706	0.0416	0.1109	0.0395	0.0317	0.2354	0.2888	0.3115	0.4220	0.3811	0.4695	0.5809	0.5424	0.6119	0.4920	0.6204	0.8259
0.9731	0.8311	0.5704	0.3346	0.1706	0.0416	0.1109	0.0395	0.0317	0.2354	0.2888	0.3115	0.4220	0.3811	0.4695	0.5809	0.5424	0.6119	0.4920	0.6204	0.8259
1.0000	0.7578	0.5573	0.3517	0.0702	0.0011	0.0698	0.0215	0.0186	0.1727	0.2619	0.2379	0.3522	0.3259	0.4064	0.5218	0.5256	0.6298	0.5357	0.6330	0.8497
1.0000	0.7578	0.5573	0.3517	0.0702	0.0011	0.0698	0.0215	0.0186	0.1727	0.2619	0.2379	0.3522	0.3259	0.4064	0.5218	0.5256	0.6298	0.5357	0.6330	0.8497
1.0000	0.7634	0.5394	0.2995	0.0937	0.0027	0.1141	0.0636	0.1051	0.2278	0.2890	0.2806	0.3664	0.3349	0.3759	0.4645	0.4807	0.5480	0.4356	0.5040	0.7579
1.0000	0.7883	0.5337	0.2777	0.0577	0.0148	0.1159	0.1201	0.1514	0.2522	0.2576	0.2434	0.3662	0.3941	0.4572	0.5943	0.6018	0.6846	0.5760	0.6430	0.9168
0.7259	0.5754	0.3927	0.2238	0.0540	0.0152	0.0877	0.0681	0.0699	0.1258	0.1878	0.1954	0.3274	0.4691	0.4678	0.5393	0.6296	0.7993	0.7684	0.7971	0.9991
0.7259	0.5754	0.3927	0.2238	0.0540	0.0152	0.0877	0.0681	0.0699	0.1258	0.1878	0.1954	0.3274	0.4691	0.4678	0.5393	0.6296	0.7993	0.7684	0.7971	0.9991
0.8001	0.5888	0.4005	0.2239	0.0423	0.0169	0.0923	0.0798	0.0750	0.1467	0.1861	0.1414	0.2635	0.3869	0.3987	0.4741	0.5743	0.7721	0.7270	0.8174	0.9979
0.8001	0.5888	0.4005	0.2239	0.0423	0.0169	0.0923	0.0798	0.0750	0.1467	0.1861	0.1414	0.2635	0.3869	0.3987	0.4741	0.5743	0.7721	0.7270	0.8174	0.9979
0.7955	0.5878	0.4237	0.2461	0.0517	0.0170	0.0838	0.0875	0.0755	0.1234	0.1740	0.1423	0.2556	0.3696	0.4177	0.5058	0.6067	0.7945	0.7498	0.7831	1.0000
0.7955	0.5878	0.4237	0.2461	0.0517	0.0170	0.0838	0.0875	0.0755	0.1234	0.1740	0.1423	0.2556	0.3696	0.4177	0.5058	0.6067	0.7945	0.7498	0.7831	1.0000
0.8838	0.7327	0.5044	0.2694	0.0547	0.0372	0.0955	0.0333	0.0013	0.0732	0.1113	0.0927	0.2277	0.2633	0.3637	0.4916	0.5827	0.7223	0.6907	0.7190	0.9962
0.8838	0.7327	0.5044	0.2694	0.0547	0.0372	0.0955	0.0333	0.0013	0.0732	0.1113	0.0927	0.2277	0.2633	0.3637	0.4916	0.5827	0.7223	0.6907	0.7190	0.9962
0.8838	0.7327	0.5044	0.2694	0.0547	0.0372	0.0955	0.0333	0.0013	0.0732	0.1113	0.0927	0.2277	0.2633	0.3637	0.4916	0.5827	0.7223	0.6907	0.7190	0.9962
0.7388	0.5630	0.3748	0.1903	0.0251	0.0105	0.1019	0.0757	0.0583	0.1176	0.1620	0.1528	0.2837	0.4102	0.4542	0.5335	0.6076	0.7736	0.7210	0.7679	0.9996

Each row of the data represents one feature vector with 21 elements. The laser-induced auto-fluorescence spectrum data between 500 and 700 nm are selected and normalized to the range between 0 and 1. One data point is picked up for every 10 nm in the wavelength, which results in the dimension of a feature vector to be 21.

References

[1] World Health Organization. Home News Fact sheets Detail Cancer, April 16, 2018.

[2] Fu S, Chia TC, Kwek LC, *et al*. Comparison of human colorectal normal tissue with cancerous tissue autofluorescence image by optical sectioning with a confocal laser-scanning microscope. In: Wilson T, ed. Confocal, Multiphoton, and Nonlinear Microscopic Imaging (Vol 5139 of Proc SPIE). Munich, Germany: Optical Society of America; 2003: p. 5139_199.

[3] Fu S, Kwek L-C, Chia T-C, *et al*. Detection of colorectal cancer using time-resolved autofluorescence spectrometer. Proc. SPIE 6191, Biophotonics and New Therapy Frontiers, 61910M. 2006; doi:10.1117/12.663257.

[4] Chia TC, Fu S, Chia YH, *et al*. Application of laser-induced autofluorescence spectra detection system in human colorectal cancer in-vivo screening. Proc. SPIE 5969, Photonic Applications in Biosensing and Imaging, 59691I. 2005; doi: 10.1117/12.632130.

[5] Kwek LC, Fu S, Chia TC, *et al*. High-sensitivity and specificity of laser-induced autofluorescence spectra for detection of colorectal cancer with an artificial neural network. Appl Opt 2005;44:4004–8.

[6] Agha RA, Borrelli MR, Farwana R, *et al*. The PROCESS 2018 statement: Updating Consensus Preferred Reporting Of CasE Series in Surgery (PROCESS) guidelines. Int J Surg 2018;60:279–82.

[7] Li M, Lu Y. Maximum likelihood DOA estimation in unknown colored noise fields. IEEE Trans Aerosp Electron Syst 2008;44:1079–90.

[8] Li M, Lu Y. A refined genetic algorithm for accurate and reliable DOA estimation with a sensor array. Wireless Pers Commun 2007;43:533–47.

[9] Li M, Lu Y. Improving the performance of GA-ML DOA estimator with a resampling scheme. Signal Process 2004;84:1813–22.

[10] Samarasinghe S. Neural Networks for Applied Sciences and Engineering: From Fundamentals to Complex Pattern Recognition, 1st ed. New York, NY: Auerbach Publications; 2007.